ACS APPLIED MATERIALS & INTERFACES

Research Article

www.acsami.org

Facile Photochemical Synthesis of Au/Pt/g-C_3N_4 with Plasmon-Enhanced Photocatalytic Activity for Antibiotic Degradation

Jinjuan Xue,[†,‡,§] Shuaishuai Ma,[†,‡,§] Yuming Zhou,[*,†,‡] Zewu Zhang,[†,‡] and Man He[†,‡]

[†]School of Chemistry and Chemical Engineering, Southeast University, Nanjing 211189, People's Republic of China

[‡]Jiangsu Optoelectronic Functional Materials and Engineering Laboratory, Nanjing 211189, People's Republic of China

ABSTRACT: A novel plasmonic photocatalyst, Au/Pt/g-C_3N_4, was prepared by a facile calcination-photodeposition technique. The samples were characterized by X-ray diffraction, energy-dispersive spectroscopy, transmission electron microscopy, and UV−vis diffuse reflectance spectroscopy, and the results demonstrated that the Au and Pt nanoparticles (7−15 nm) were well-dispersed on the surfaces of g-C_3N_4. The Au/Pt codecorated g-C_3N_4 heterostructure displayed enhanced photocatalytic activity for antibiotic tetracycline hydrochloride (TC-HCl) degradation, and the degradation rate was 3.4 times higher than that of pure g-C_3N_4 under visible light irradiation. The enhancement of photocatalytic activity could be attributed to the surface plasmon resonance effect of Au and electron-sink function of Pt nanoparticles, which improve the optical absorption property and photogenerated charge carriers separation of g-C_3N_4, synergistically facilitating the photocatalysis process. Finally, a possible photocatalytic mechanism for degrading TC-HCl by Au/Pt/g-C_3N_4 heterostructure was tentatively proposed.

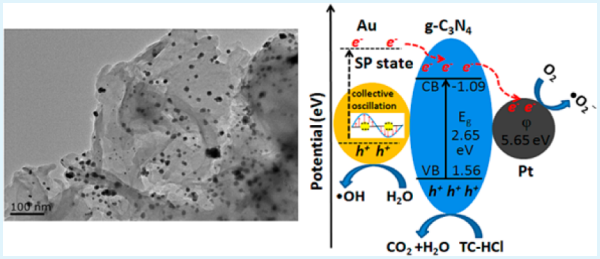

KEYWORDS: *plasmonic photocatalyst, Au/Pt/g-C_3N_4, visible light, photocatalytic activity*

INTRODUCTION

Recently, the presence of pharmaceutical residues in wastewater and their harmful effects on living ecosystems have aroused worldwide attention. Pharmaceutical residues are discharged into the aquatic environment through various sources such as pharmaceutical industry, hospital effluent, and excretion from humans and livestock,[1] causing pollution of the living environment. Antibiotic residues account for a large proportion of the pharmaceutical contaminations because antibiotics have a high consumption rate in not only humans but also in aquaculture and livestock medicines.[2] Antibiotic residues in aqueous systems have the potential to induce negative environmental effects, even in low concentrations, including antibiotic resistance to bacteria, perturbations in ecosystems, and possible risks to human health through drinking water and the food chain.[3−6] Several techniques such as activated carbon adsorption, microbial degradation, and electrolysis have been applied to deal with antibiotic residues.[7] Moreover, semiconductor mediated photocatalysis has become the focus of recent research on antibiotic residue treatment because it is a green, efficient technology, compared to conventional techniques. Some studies have already been carried out in this area, such as photocatalytic degradation of tetracycline by nonthermal plasma combined with nano-TiO_2,[8] TiO_2/5A composite photocatalyst degrading antibiotic oxytetracycline,[9] degradation of ceftiofur sodium using Au-TiO_2 photocatalyst,[10] and so on. Graphitic carbon nitride (g-C_3N_4) is a polymeric metal-free semiconductor with a medium band gap (2.65 eV), and it possesses a two-dimensional layered structure by the sp^2 hybridization of carbon and nitrogen forming the π-conjugated graphitic planes.[11] g-C_3N_4 has attracted tremendous attention for applications in photocatalytic field such as photodegradation of a variety of pollutions, hydrogen production by water splitting, and photocatalytic reduction of CO_2 owing to its unique properties, such as physicochemical stability, response to visible light, easy preparation via cheap materials, and environmental friendliness.[12−16] Nevertheless, the shortcomings of low visible light utilization efficiency and fast recombination of photogenerated electron−hole pairs in pure g-C_3N_4 still limit the further improvement of its photocatalytic activity. Therefore, some approaches have been employed to enhance the photocatalytic activity of g-C_3N_4, such as nano/mesoporous structures design,[17−19] doping with metal or nonmetal elements,[20,21] surface modification,[22−24] heterostructured nanocomposites fabrication,[25−29] and so forth.

The surface plasmon resonance (SPR) effect of noble metals derived from the collective coherent oscillation of surface electrons enables noble metals nanoparticles (NPs) to be a promising candidate for harvesting both UV light and visible light.[30−32] Consequently, noble metal−semiconductor composites have been widely developed to function as effective visible-light-induced plasmonic photocatalysts. For instance, the Au/TiO_2 system[33−35] and the Ag/AgX (X = Cl, Br) system[36] have been well exploited to be such plasmonic photocatalysts. In these systems, the novel metal NPs could be regarded as efficient media to absorb light, then the hot electrons generated

Received: February 9, 2015
Accepted: April 20, 2015
Published: April 20, 2015

DOI: 10.1021/acsami.5b01212
ACS Appl. Mater. Interfaces 2015, 7, 9630−9637

on the NPs gain light energy and further migrate to the conduction band of the semiconductor.[37] In addition, the combination of two different novel metal NPs has shown excellent bimetallic co-effect for many important reactions in the catalysis field.[38,39]

Herein, for the first time, we demonstrate a simple calcination-photodeposition technique to fabricate bimetallic Au and Pt NPs codecorated g-C_3N_4 (denoted as Au/Pt/g-C_3N_4) plasmonic photocatalyst. The photocatalytic performance of the sample was investigated by photodegradation of antibiotic residue tetracycline hydrochloride (TC-HCl), as expected, the obtained Au/Pt/g-C_3N_4 showed enhanced photocatalytic activity over that of Au/g-C_3N_4, Pt/g-C_3N_4, and pure g-C_3N_4 under visible light irradiation. Coupling both of the Au and Pt NPs with g-C_3N_4, the Au/Pt/g-C_3N_4 nanocomposites can improve the optical adsorption ability as well as promote photogenerated electron−hole pairs separation, which were beneficial from Au NPs SPR effect and Pt NPs electron-sink function.

EXPERIMENTAL SECTION

Synthesis of g-C_3N_4. The g-C_3N_4 power was synthesized by one-step polymerization of 5 g of melamine according to the literature.[40] In a typical procedure, the precursor melamine was thermally treated in a tube furnace at 550 °C for 4 h with a heating rate of 2 °C/min under air atmosphere. The yellow-colored product was collected and ground into powder for further use.

Synthesis of Au/Pt/g-C_3N_4 Plasmonic Photocatalyst. Au and Pt NPs codecorated g-C_3N_4 nanocomposites were prepared through a photodeposition procedure with hole scavenger (PH) method. Generally, 0.5 g of the as-prepared g-C_3N_4 power was dispersed in 100 mL of deionized water with ultrasonication, and 2.3 mL of isopropanol was added to act as a hole scavenger. Then, 1 mL of $HAuCl_4$ (10 mg/mL Au) and 430 μL of K_2PtCl_4 (5.875 mg/mL Pt) aqueous solutions were added into the above suspension, and the mixture was stirred for 30 min. The calculated amounts of the deposited Au and Pt were 2.0 and 0.5% weight total to g-C_3N_4, respectively. With continuous nitrogen sparging, the suspension was photoirradiated for 3 h by a mercury arc lamp (250 W, GY-250, λ = 365 nm) under magnetic stirring. The codecorated Au (III) and Pt (II) salt sources were reduced by photogenerated electrons, and the novel metals were deposited on the surfaces of the g-C_3N_4. The solid product was collected by centrifugation and washed with distilled water for several times, and dried at 80 °C overnight to obtain the Au/Pt/g-C_3N_4 nanocomposites. The Au/g-C_3N_4 (Au 2.0 wt %) and Pt/g-C_3N_4 (Pt 0.5 wt %) were also prepared by using the same method as the control samples for comparison.

Sample Characterizations. X-ray diffraction (XRD) measurements were performed on a SmartLab XRD spectrometer (Rigaku) with Cu Kα radiation in the range of 10−70° (2θ). Scanning electron microscope (SEM) images were obtained with a FEI Inspect F50 field-emission scanning electron microscope. Transmission electron microscopy (TEM) and high-resolution TEM (HRTEM) images were taken with a JEM-2100 high-resolution transmission electron microscope. X-ray photoelectron spectroscopy (XPS) analysis was carried out on a Kratos Axis Ultra DLD spectrometer equipped with a monochromatic Al Kα X-ray source (1486.6 eV). UV−vis diffuse reflectance spectroscopy (DRS) was performed using a UV−vis spectrophotometer (UV-3600, Shimadzu) with an integrating sphere attachment. PL spectra were measured at room temperature on a Shimadzu RF-5301 fluorescence spectrophotometer with 385 nm excitation wavelength.

Photocatalytic Activity Test. The typical photocatalytic experiment was carried in a Pyrex reactor with reflux water at room temperature. The photocatalytic activities of the as-prepared samples were evaluated by the photodegradation of TC-HCl under visible light irradiation. In the experiment, the photocatalyst (100 mg) was dispersed in 100 mL of TC-HCl aqueous solution (20 mg/L), and the mixed suspension was magnetically stirred for 30 min in the dark to obtain absorption−desorption equilibrium before irradiation. Subsequently, the above suspension was irradiated by a 500 W xenon lamp (Philips) with a 400 nm cutoff filter, which was employed for the light source. At 30 min intervals, 3 mL of suspension was sampled and filtered through a 0.45 μm PTFE syringe filter to remove the solid particles and obtain clear liquid. The concentrations of TC-HCl in the liquid were analyzed by a UV−vis spectrophotometer (UV-3600; Shimadzu). For comparison, the photocatalytic experiments of the Au/g-C_3N_4 and Pt/g-C_3N_4 were also carried out under identical conditions.

RESULTS AND DISCUSSION

Structure and Morphology. The XRD patterns of the as-prepared g-C_3N_4, Pt/g-C_3N_4, Au/g-C_3N_4, and Au/Pt/g-C_3N_4 nanocomposites are shown in Figure 1. As can be seen, the

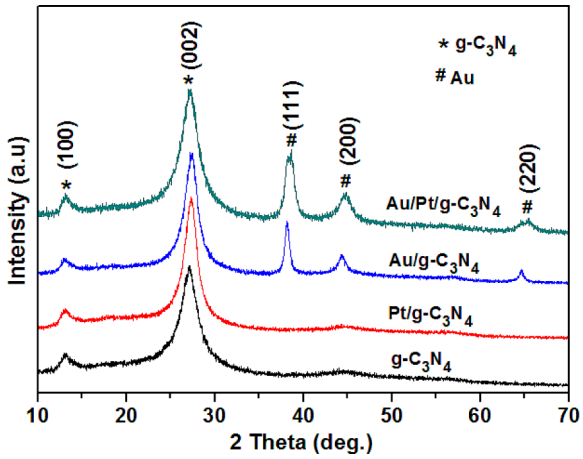

Figure 1. XRD patterns of the as-prepared g-C_3N_4, Pt/g-C_3N_4, Au/g-C_3N_4, and Au/Pt/g-C_3N_4 nanocomposites.

pure g-C_3N_4 shows one diffraction peak of (100) plane at about 2θ = 13.1° with respect to the characteristic interlayer structural packing, and another diffraction peak of (002) plane at 27.2° corresponding to the interplanar stacking peaks of the aromatic systems.[41,42] Compared with pure g-C_3N_4, the Au/g-C_3N_4 and Au/Pt/g-C_3N_4 samples exhibit three additional peaks at 38.2, 44.4, and 64.6°, which are indexed to the (111), (200), and (220) planes of Au, respectively. Such observations indicated that the Au NPs were successfully loaded on the g-C_3N_4 after irradiation.[43] Nevertheless, the diffraction peaks of Pt were not detected in the samples of Pt/g-C_3N_4 and Au/Pt/g-C_3N_4, which may be due to its low loading content and high dispersity.

Figure 2 depicts the FESEM images of the Au/Pt/g-C_3N_4 nanocomposites. As can be seen, the aggregated edge of g-C_3N_4 displays two-dimensional (2D) lamellar structures and an amount of nanoparticles are attached to the surfaces of g-C_3N_4. In spite of the difficulty to differentiate the composition of every nanoparticle, we can reveal it in the following characterization. The morphologies and microstructures of g-C_3N_4 and Au/Pt/g-C_3N_4 nanocomposites were further investigated by TEM and HRTEM (Figure 3). As shown in Figure 3a, g-C_3N_4 possessed a layered structure, and it presents in the form of a thin sheet with irregular morphology. After UV-light irradiation of the g-C_3N_4 in the presence of Au (III) and Pt (II) salts, the regularly shaped spherical Au and Pt NPs sized 7−15 nm uniformly generated on the surfaces of g-C_3N_4

DOI: 10.1021/acsami.5b01212
ACS Appl. Mater. Interfaces 2015, 7, 9630−9637

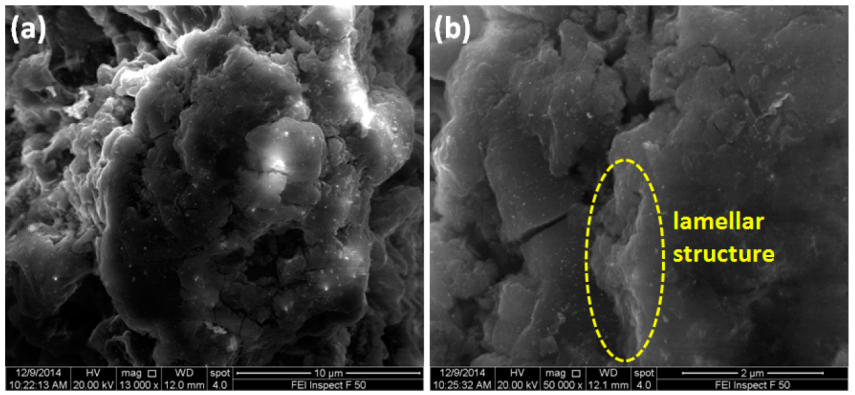

Figure 2. FESEM images of the Au/Pt/g-C_3N_4 nanocomposites at (a) low magnification and (b) high resolution.

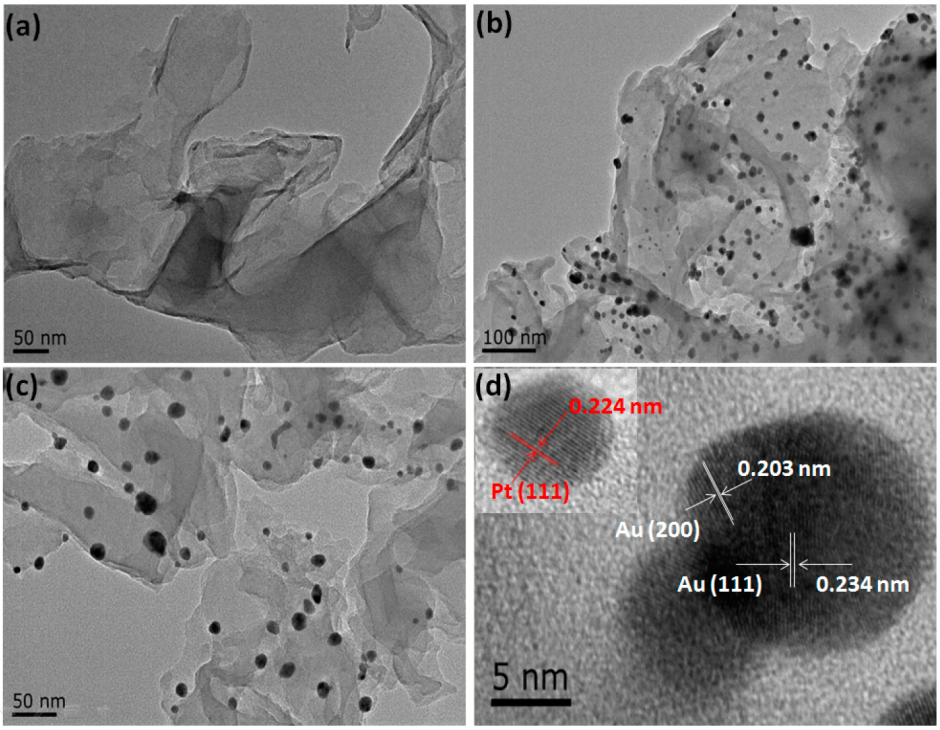

Figure 3. Typical TEM images of (a) g-C_3N_4 and (b and c) Au−Pt−C_3N_4 nanocomposites. (d) HRTEM image of the as-prepared Au−Pt−C_3N_4 nanocomposites.

to form the Au/Pt/g-C_3N_4 structure, which is shown in Figure 3b,c. Furthermore, the interplanar distances of 0.234, 0.203, and 0.224 nm measured out in the HRTEM image (Figure 3d) are well indexed to the lattice spacing of the Au (111), Au (200), and Pt (111) planes, respectively.[44] All of the above observations indicated that the Au−Pt codecorated g-C_3N_4 heterostructure (Au/Pt/g-C_3N_4) was indeed formed.

The XPS spectra were employed to analyze the detailed chemical status of the sample. As observed from Figure 4a, the C 1s spectrum can be fitted into three peaks at binding energies of 284.4, 285.5, and 287.8 eV, which are attributed to pure graphitic sites in the carbon nitride matrix (C−C), the sp^2-hybridized carbon atoms bonded to N in an aromatic ring (C−N−C) and the sp^2-hybridized carbon in the aromatic ring attached to the NH_2 group ($C-(N)_3$).[41,45−47] The N 1s spectrum in Figure 4b can be deconvoluted into three peaks, ascribable to C−N−C at 397.7 eV, $N-(C)_3$ at 398.6 eV, and N−H at 400.1 eV.[46,47] The Au 4f spectra spectrum (Figure 4c) consists of two peaks with binding energies of 83.7 and 87.5 eV for Au $4f_{7/2}$ and Au $4f_{5/2}$, respectively, well in agreement with the Au^0 state values.[48] The peaks at binding energy values of 72.5 and 75.7 eV for Pt $4f_{7/2}$ and $4f_{5/2}$ were observed in the Pt 4f spectra spectrum of Figure 4d, corresponding to the standard binding energy values of Pt^0 state.[49,50]

The UV−vis diffuse reflectance spectra of g-C_3N_4, Pt/g-C_3N_4, Au/g-C_3N_4, and Au/Pt/g-C_3N_4 samples are demonstrated in Figure 5. As can be seen, pure g-C_3N_4 displayed an absorption band lower than about 460 nm, resulting in a low visible light utilization efficiency, whereas both of the Au/g-C_3N_4 and Au/Pt/g-C_3N_4 samples exhibit a broad absorption peak at around 550 nm which could be attributed to the SPR effect of Au NPs.[51] Meanwhile, we observed a significant enhancement of optical absorption in the visible light region, ascribable to the plasmonic resonance of Au NPs aroused from the collective oscillations of the hot electrons generated on the irradiated Au NPs.[52,53] Nevertheless, the SPR of Pt NPs cannot be observed due to the high imaginary part of the dielectric function of Pt.[54] Benefiting from such enlarged light absorption

DOI: 10.1021/acsami.5b01212
ACS Appl. Mater. Interfaces 2015, 7, 9630−9637

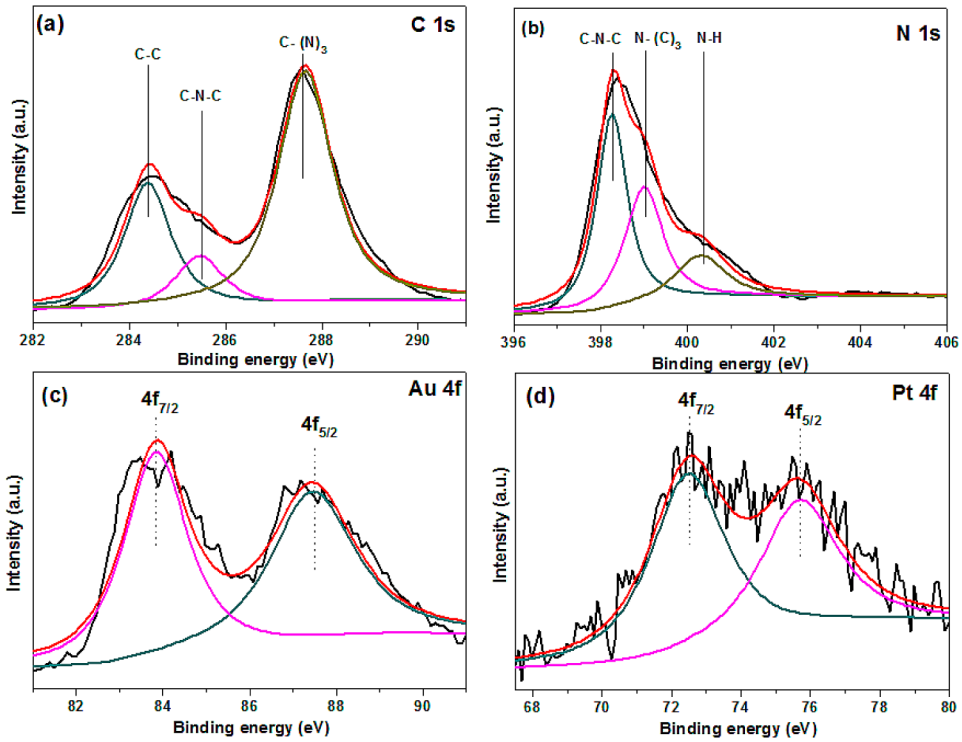

Figure 4. XPS spectra of (a) C 1s, (b) N 1s, (c) Au 4f, and (d) Pt 4f of the as-prepared Au/Pt/g-C_3N_4 nanocomposites.

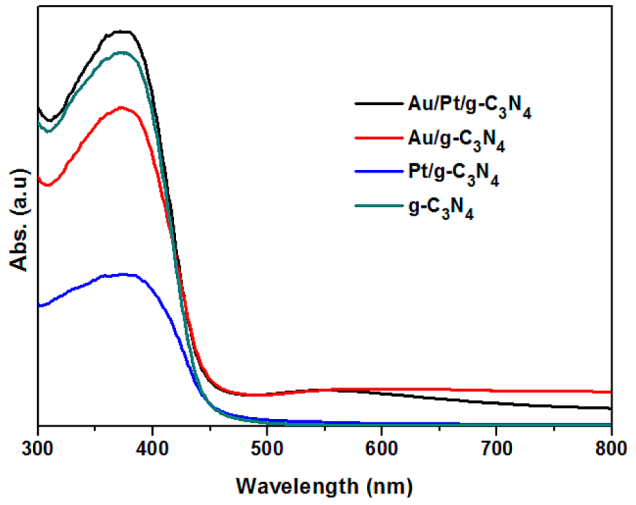

Figure 5. UV−vis diffuse reflectance spectra of g-C_3N_4, Pt/g-C_3N_4, Au/g-C_3N_4, and Au/Pt/g-C_3N_4 nanocomposites.

range and intensity, the Au/Pt/g-C_3N_4 plasmonic photocatalyst is expected to enhance the solar energy utilization efficiency in the photocatalysis process, showing improved visible-light-driven photocatalytic performance.

Photocatalytic Performance. Tetracyclines (TCs) represent a major proportion of the antibiotics currently in use,[55] and tetracycline hydrochloride (TC-HCl) was chosen as a hazardous representative to evaluate the photocatalytic performances of the as-prepared photocatalysts. Figure 6a shows the photocatalytic activities of g-C_3N_4, Pt/g-C_3N_4, Au/g-C_3N_4, and Au/Pt/g-C_3N_4 samples in degradation of TC-HCl under visible light irradiation. The blank experiment demonstrates that the direct photolysis of TC-HCl can be ignored because TC-HCl is only slightly degraded without photocatalyst after visible light irradiated for 3 h. And it can seen from Figure 6a that the degradation rate of TC-HCl follows an order of Au/Pt/g-C_3N_4 (93.0%) > Au/g-C_3N_4 (78.6%) > Pt/g-C_3N_4 (67.2%) > g-C_3N_4 (52.8%) after the same irradiation time.

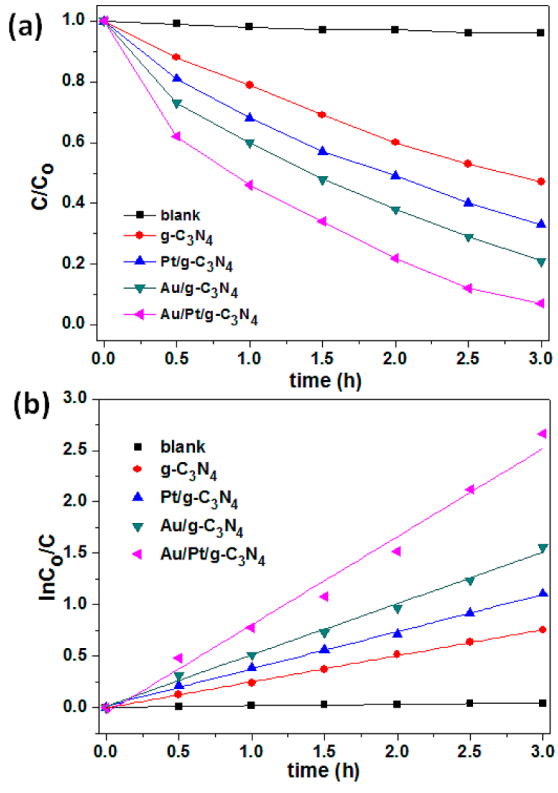

Figure 6. (a) Photocatalytic activities and (b) kinetics of the as-prepared g-C_3N_4, Pt/g-C_3N_4, Au/g-C_3N_4, and Au/Pt/g-C_3N_4 nanocomposites for degradation of TC-HCl under visible light irradiation.

DOI: 10.1021/acsami.5b01212
ACS Appl. Mater. Interfaces 2015, 7, 9630−9637

Therefore, it is easy to conclude that the degradation efficiency of TC-HCl can be improved in the presence of Au loaded g-C_3N_4 and Pt loaded g-C_3N_4 photocatalytic systems as compared to pure g-C_3N_4, particularly remarkably enhanced with the Au/Pt codecorated g-C_3N_4 photocatalyst. The phenomenon also implied that the bimetallic decoration was advantageous than monometallic decoration, which was resulted from the synergistic effect between Au and Pt accounting for the significant enhancement of the photocatalytic activity. Moreover, the photocatalytic degradation of the organic pollutant generally can be regarded as a pseudo-first-order kinetics reaction when C_o is within the millimolar concentration range.[56]

$$\ln(C_o/C) = kt$$

where C_o is the concentration of TC-HCl after initial adsorption−desorption equilibrium, C is the concentration after visible light irradiation, and k is the first-order kinetics rate constant. The linear relationship between $\ln(C_o/C)$ and t are depicted in Figure 6(b). After calculated, the rate constants of g-C_3N_4, Pt/g-C_3N_4, Au/g-C_3N_4 and Au/Pt/g-C_3N_4 samples are 0.1269 min^{-1}, 0.1809 min^{-1}, 0.2495 min^{-1}, and 0.4286 min^{-1}, respectively. Obviously, Au/Pt/g-C_3N_4 exhibits the best degradation efficiency and has the highest rate constant among the above four samples, giving a 3.4 times higher rate constant of TC-HCl degradation than pure g-C_3N_4. The excellent photocatalytic performance for the Au/Pt/g-C_3N_4 sample, on one hand, should be largely attributed to the SPR effect of Au NPs induced broadband optical absorption enhancement.[51−53] On the other hand, it could be ascribable to the loaded Pt NPs served as an electron tank to facilitate charge carriers separation and accept the separated photogenerated electrons.[44]

Because a photocatalyst's practical application also requires it is renewable besides its catalytic activity, we carried out four cycling tests to degrade TC-HCl using the as-prepared Au/Pt/g-C_3N_4 photocatalyst to investigate its stability, as shown in Figure 7. The Au/Pt/g-C_3N_4 sample for photocatalytic decomposition of TC-HCl shows a slight decline rather than a significant loss of activity after four cycles, where the photocatalytic efficiency reduces only 8.7%, suggesting the photocatalyst is stable.

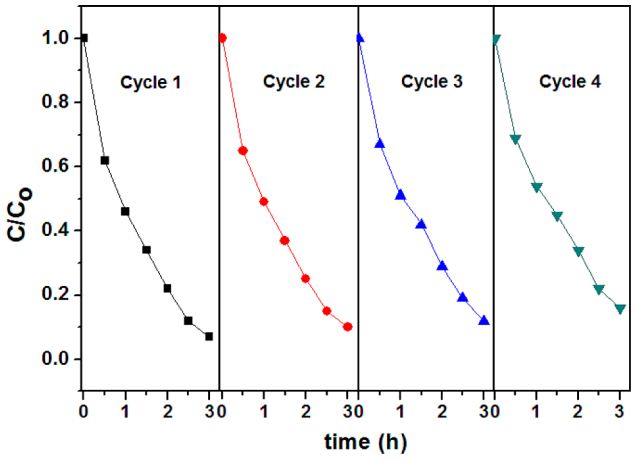

Figure 7. Four photocatalytic degradation cycles of TC-HCl by Au/Pt/g-C_3N_4 under visible light irradiation.

Proposed Mechanism for Enhanced Photocatalytic Activity. On the basis of the analysis discussed above, we proposed a possible mechanism of degradation of TC-HCl by visible-light-driven Au/Pt/g-C_3N_4 photocatalyst; it is presented in Figure 8. Under visible light irradiation, both the Au SPR and

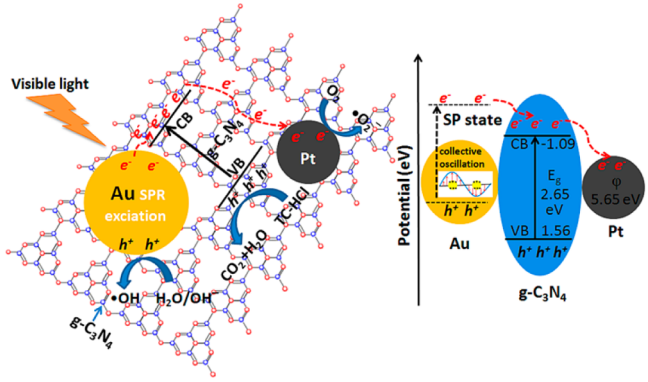

Figure 8. Proposed photocatalytic mechanism for degradation of TC-HCl by Au/Pt/g-C_3N_4 nanocomposites under visible light irradiation.

g-C_3N_4 could be excited. As reported by Zhang et al., when the novel metal SPR combined with the excited semiconductors under irradiation, it is possible to achieve a synergic effect which would take an important place in plasmon-related photocatalysis processes.[57] In our study, SPR-excitation of Au NPs generated hot electron−hole pairs, and the hot electrons transiently occupied empty states in the Au conduction band (CB) above the Fermi energy, further energetically injected to the CB of g-C_3N_4, with the hot holes left on Au NPs.[35,58,59] It is known that the photoexcited semiconductor exhibits higher conductivity due to more charge carriers are created in the structure by the excitation.[60,61] Therefore, g-C_3N_4 could serve as a excellent mediator for the rapid transport of the hot electrons to the nearby Pt NPs. As to g-C_3N_4, electrons (e^-) in the valence band (VB) were excited to the CB with the simultaneous generation of holes (h^+) in the VB. With the hot electrons by SPR excitation injected, the nonequilibrated electrons on the CB of g-C_3N_4 then transferred to the Pt NPs. Such electrons transfer direction is feasible because the CB of g-C_3N_4 (−1.09 eV) is lower than the work function of Pt (5.65 eV).[62] In this case, the photogenerated charge carrier separation was boosted, and the transportation process was accelerated to some extent. A majority of photogenerated electrons (e^-) that transferred on Pt NPs can react with O_2 to generate active species $\cdot O_2^-$, while photogenerated holes (h^+) left on the Au NPs simultaneously reacted with H_2O or OH^- to produce active species such as ·OH. Moreover, because the E_{VB} value of g-C_3N_4 (+1.57 eV vs SHE) is lower than the standard redox potentials of $\cdot OH/H_2O$ (+2.68 eV vs SHE) and $\cdot OH/OH^-$ (+1.99 V vs SHE), photogenerated holes (h^+) left on the VB of g-C_3N_4 could not react with H_2O or OH^- to generate the active oxidative species ·OH,[63,64] hence h^+ on the VB of g-C_3N_4 would be consumed by directly decomposing TC-HCl. The major routes of photocatalytic degradation of TC-HCl under visible-light irradiation were proposed as follows:

$$Au + h\nu \rightarrow Au(e^- + h^+)$$

$$g\text{-}C_3N_4 + h\nu \rightarrow g - C_3N_4(e^- + h^+)$$

$$Au(e^-)/g - C_3N_4(e^-) + Pt \rightarrow Au/g - C_3N_4 + Pt(e^-)$$

DOI: 10.1021/acsami.5b01212
ACS Appl. Mater. Interfaces 2015, 7, 9630−9637

$$Pt(e^-) + O_2 \rightarrow Pt + \cdot O_2^-$$

$$\cdot O_2^- + H_2O \rightarrow \cdot OH + HO_2\cdot$$

$$Au(h^+) + H_2O \rightarrow \cdot OH + H^+$$

$$\cdot O_2^- + H^+ \rightarrow HO_2\cdot$$

$$2HO_2\cdot \rightarrow H_2O_2 + O_2$$

$$H_2O_2 + \cdot O_2^- \rightarrow \cdot OH + OH^- + O_2$$

$$Au(h^+) + OH^- \rightarrow Au + \cdot OH$$

$$\cdot OH + TC - HCl \rightarrow \text{degradation products}$$

$$g\text{-}C_3N_4(h^+) + TC - HCl \rightarrow \text{degradation products}$$

PL quenching effect is related to the transfer and recombination processes of charge carries in the photocatalysts, so it is an efficient method to apply PL spectral analysis to investigate the recombination rate of photogenerated electron−hole pairs. It was generally believed that a lower PL emission intensity is an indication of a lower recombination of photogenerated electron−hole pairs.[63] Figure 9 shows the PL spectra of pure g-C_3N_4, Pt/g-C_3N_4, Au/g-C_3N_4, and Au/Pt/g-C_3N_4 samples at an excitation wavelength of 385 nm. The four samples all have the same wide emission peaks at about 460 nm, which could be attributed to the band gap recombination of photoexcited electron−hole pairs in g-C_3N_4.[65] As can be observed, the PL emission intensities of Pt/g-C_3N_4 and Au/g-C_3N_4 decreased compared to that of pure g-C_3N_4, while Au/Pt codecorated g-C_3N_4 exhibited a further decrease in PL emission intensity. It is suggested that the recombination extent of the photogenerated electron−hole pairs was inhibited more greatly in Au/Pt/g-C_3N_4 photocatalyst, which would contribute to the enhancement of photocatalytic efficiency.

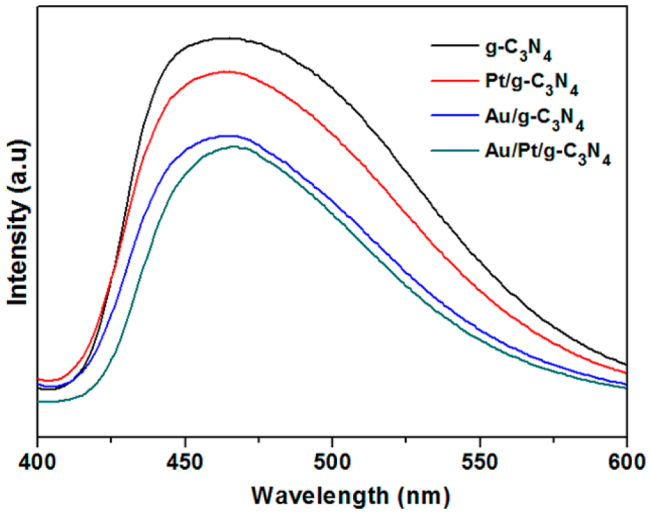

Figure 9. PL emission spectra of pure g-C_3N_4, Pt/g-C_3N_4, Au/g-C_3N_4, and Au/Pt/g-C_3N_4 samples.

CONCLUSIONS

In summary, we have successfully fabricated Au/Pt codecorated g-C_3N_4 heterostructure as a plasmonic photocatalyst by using a simple calcination-photodeposition technique. Au and Pt NPs with size of 7−15 nm were deposited onto the surfaces of g-C_3N_4. The obtained Au/Pt/g-C_3N_4 nanocomposites displayed improved degradation efficiency of TC-HCl compared to pure g-C_3N_4 under visible light irradiation. The Au SPR effect that enlarged the optical adsorption range combining with the electron-sink function of Pt to efficiently separate photogenerated charge carriers synergistically account for the enhancement of photocatalytic activity. Besides, hydrogen evolution through water splitting by such Au/Pt/g-C_3N_4 photocatalyst is theoretically feasible and under further investigation. In all, Au/Pt/g-C_3N_4 plasmonic photocatalyst has potential application in solving the problems of worldwide environmental pollution and energy crisis by efficiently utilizing solar energy.

AUTHOR INFORMATION

Corresponding Author

*Tel.: +86 25 52090617. Fax: +86 25 52090617. E-mail: ymzhou@seu.edu.cn.

Author Contributions

§These authors contributed equally to this work.

Notes

The authors declare no competing financial interest.

ACKNOWLEDGMENTS

The authors are grateful to the financial support of the National Natural Science Foundation of China (Grant Nos. 21376051, 21306023, and 21106017), the Natural Science Foundation of Jiangsu (Grant No. BK20131288), the Fund Project for Transformation of Scientific and Technological Achievements of Jiangsu Province of China (Grant No. BA2014100), and the Fundamental Research Funds for the Central Universities (Grant No. 3207045301).

REFERENCES

(1) Elmolla, E. S.; Chaudhuri, M. Photocatalytic Degradation of Amoxicillin, Ampicillin and Aloxacillin Antibiotics in Aqueous Solution Using UV/TiO_2 and UV/H_2O_2/TiO_2 Photocatalysis. *Desalination* **2010**, *252*, 46−52.

(2) Walter, M. V.; Vennes, J. W. Occurrence of Multiple-Antibiotic-Resistant Enteric Bacteria in Domestic Sewage and Oxidation Lagoons. *Appl. Environ. Microbiol.* **1985**, *50*, 930−933.

(3) Trovo, A. G.; Nogueira, R. F. P.; Aguera, A.; Fernandez-Alba, A. R.; Malato, S. Degradation of the Antibiotic Amoxicillin by Photo-Fenton Process—Chemical and Toxicological Assessment. *Water. Res.* **2011**, *45*, 1394−1402.

(4) Phan, T. P. H.; Managaki, S.; Nakada, N.; Takada, H.; Shimizu, A.; Anh, D. H.; Viet, P. H.; Suzuki, S. Antibiotic Contamination and Occurrence of Antibiotic-Resistant Bacteria in Aquatic Environments of Northern Vietnam. *Sci. Total Environ.* **2011**, *409*, 2894−2901.

(5) Homem, V.; Alves, A.; Santos, L. Amoxicillin Degradation at ppb Levels by Fenton's Oxidation Using Design of Experiments. *Sci. Total Environ.* **2010**, *408*, 6272−6280.

(6) Lee, Y. J.; Lee, S. E.; Lee, D. S.; Kim, Y. H. Risk Assessment of Human Antibiotics in Korean Aquatic Environment. *Environ. Toxicol. Pharmacol.* **2008**, *26*, 216−221.

(7) Yu, X. N.; Gao, X.; Lu, Z. Y.; Liu, X. L.; Huo, P. W.; Liu, X. L.; Wu, D.; Yan, Y. S. Preparation and Photodegradation Properties of Transition Metal Ion−Poly-*o*-phenylenediamine/TiO_2/Fly-Ash Cenospheres by Ion ImprintingTechnology. *RSC Adv.* **2013**, *3*, 14807−14813.

(8) He, D.; Sun, Y. B.; Xin, L.; Feng, J. W. Aqueous Tetracycline Degradation by Non-Thermal Plasma Combined with Nano-TiO_2. *Chem. Eng. J.* **2014**, *258*, 18−25.

(9) Zhao, C.; Zhou, Y.; de Ridder, D. J.; Zhai, J.; Wei, Y. M.; Deng, H. P. Advantages of TiO_2/5A Composite Catalyst for Photocatalytic

DOI: 10.1021/acsami.5b01212
ACS Appl. Mater. Interfaces 2015, 7, 9630−9637

Degradation of Antibiotic Oxytetracycline in Aqueous Solution: Comparison between TiO_2 and TiO_2/5A Composite System. *Chem. Eng. J.* **2014**, *248*, 280−289.
(10) Pugazhenthiran, N.; Murugesan, S.; Sathishkurnar, P.; Anandan, S. Photocatalytic Degradation of Ceftiofur Sodium in the Presence of Gold Nanoparticles Loaded TiO_2 under UV−Visible Light. *Chem. Eng. J.* **2014**, *241*, 401−409.
(11) Thomas, A.; Fischer, A.; Goettmann, F.; Antonietti, M.; Muller, J. O.; Schlogl, R.; Carlsson, J. M. Graphitic Carbon Nitride Materials: Variation of Structure and Morphology and Their Use as Metal-Free Catalysts. *J. Mater. Chem.* **2008**, *18*, 4893−4908.
(12) Zhang, X. D.; Xie, X.; Wang, H.; Zhang, J. J.; Pan, B. C.; Xie, Y. Enhanced Photoresponsive Ultrathin Graphitic-Phase C_3N_4 Nanosheets for Bioimaging. *J. Am. Chem. Soc.* **2013**, *135*, 18−21.
(13) Yang, S. B.; Gong, Y. J.; Zhang, J. S.; Zhan, L.; Ma, L. L.; Fang, Z. Y.; Vajtai, R.; Wang, X. C.; Ajayan, P. M. Exfoliated Graphitic Carbon Nitride Nanosheets as Efficient Catalysts for Hydrogen Evolution under Visible Light. *Adv. Mater.* **2013**, *25*, 2452−2456.
(14) Mao, J.; Peng, T. Y.; Zhang, X. H.; Li, K.; Ye, L. Q.; Zan, L. Effect of Graphitic Carbon Nitride Microstructures on the Activity and Selectivity of Photocatalytic CO_2 Reduction under Visible Light. *Catal. Sci. Technol.* **2013**, *3*, 1253−1260.
(15) Jorge, A. B.; Martin, D. J.; Dhanoa, M. T. S.; Rahman, A. S.; Makwana, N.; Tang, J. W.; Sella, A.; Cora, F.; Firth, S.; Darr, J. A.; McMillan, P. F. H_2 and O_2 Evolution from Water Half-Splitting Reactions by Graphitic Carbon Nitride Materials. *J. Phys. Chem. C* **2013**, *117*, 7178−7185.
(16) Dong, G. H.; Zhang, L. Z. Porous Structure Dependent Photoreactivity of Graphitic Carbon Nitride under Visible Light. *J. Mater. Chem.* **2012**, *22*, 1160−1166.
(17) Li, X. H.; Wang, X. C.; Antonietti, M. Mesoporous g-C_3N_4 Nanorods as Multifunctional Supports of Ultrafine Metal Nanoparticles: Hydrogen Generation from Water and Reduction of Nitrophenol with Tandem Catalysis in One Step. *Chem. Sci.* **2012**, *3*, 2170−2174.
(18) Niu, P.; Zhang, L. L.; Liu, G.; Cheng, H. M. Graphene-Like Carbon Nitride Nanosheets for Improved Photocatalytic Activities. *Adv. Funct. Mater.* **2012**, *22*, 4763−4770.
(19) Han, K. K.; Wang, C. C.; Li, Y. Y.; Wan, M. M.; Wang, Y.; Zhu, J. H. Facile Template-Free Synthesis of Porous g-C_3N_4 with High Photocatalytic Performance under Visible Light. *Rsc. Adv.* **2013**, *3*, 9465−9469.
(20) Liu, G.; Niu, P.; Sun, C. H.; Smith, S. C.; Chen, Z. G.; Lu, G. Q.; Cheng, H. M. Unique Electronic Structure Induced High Photoreactivity of Sulfur-Doped Graphitic C_3N_4. *J. Am. Chem. Soc.* **2010**, *132*, 11642−11648.
(21) Yue, B.; Li, Q. Y.; Iwai, H.; Kako, T.; Ye, J. H. Hydrogen Production Using Zinc-Doped Carbon Nitride Catalyst Irradiated with Visible Light. *Sci. Technol. Adv. Mater.* **2011**, *12*, 034401.
(22) Di, Y.; Wang, X. C.; Thomas, A.; Antonietti, M. Making Metal-Carbon Nitride Heterojunctions for Improved Photocatalytic Hydrogen Evolution with Visible Light. *ChemCatChem.* **2010**, *2*, 834−838.
(23) Liu, J. H.; Zhang, Y. W.; Lu, L. H.; Wu, G.; Chen, W. Self-Regenerated Solar-Driven Photocatalytic Water-Splitting by Urea Derived Graphitic Carbon Nitride with Platinum Nanoparticles. *Chem. Commun.* **2012**, *48*, 8826−8828.
(24) Samanta, S.; Martha, S.; Parida, K. Facile Synthesis of Au/g-C_3N_4 Nanocomposites: An Inorganic/Organic Hybrid Plasmonic Photocatalyst with Enhanced Hydrogen Gas Evolution under Visible-Light Irradiation. *ChemCatChem.* **2014**, *6*, 1453−1462.
(25) Sun, L. M.; Zhao, X.; Jia, C. J.; Zhou, Y. X.; Cheng, X. F.; Li, P.; Liu, L.; Fan, W. L. Enhanced Visible-Light Photocatalytic Activity of g-C_3N_4-$ZnWO_4$ by Fabricating a Heterojunction: Investigation Based on Experimental and Theoretical Studies. *J. Mater. Chem.* **2012**, *22*, 23428−23438.
(26) Liu, W.; Wang, M. L.; Xu, C. X.; Chen, S. F.; Fu, X. L. Significantly Enhanced Visible-Light Photocatalytic Activity of g-C_3N_4 via ZnO Modification and the Mechanism Study. *J. Mol. Catal. a-Chem.* **2013**, *368*, 9−15.
(27) Yan, S. C.; Lv, S. B.; Li, Z. S.; Zou, Z. G. Organic-Inorganic Composite Photocatalyst of g-C_3N_4 and TaON with Improved Visible Light Photocatalytic Activities. *Dalton Trans.* **2010**, *39*, 1488−1491.
(28) Ye, S.; Qiu, L. G.; Yuan, Y. P.; Zhu, Y. J.; Xia, J.; Zhu, J. F. Facile Fabrication of Magnetically Separable Graphitic Carbon Nitride Photocatalysts with Enhanced Photocatalytic Activity under Visible Light. *J. Mater. Chem. A* **2013**, *1*, 3008−3015.
(29) Li, Y. B.; Zhang, H. M.; Liu, P. R.; Wang, D.; Li, Y.; Zhao, H. J. Cross-Linked g-C_3N_4/rGO Nanocomposites with Tunable Band Structure and Enhanced Visible Light Photocatalytic Activity. *Small* **2013**, *9*, 3336−3344.
(30) Linic, S.; Christopher, P.; Ingram, D. B. Plasmonic-Metal Nanostructures for Efficient Conversion of Solar to Chemical Energy. *Nat. Mater.* **2011**, *10*, 911−921.
(31) Shahjamali, M. M.; Bosman, M.; Cao, S. W.; Huang, X.; Saadat, S.; Martinsson, E.; Aili, D.; Tay, Y. Y.; Liedberg, B.; Loo, S. C. J.; Zhang, H.; Boey, F.; Xue, C. Gold Coating of Silver Nanoprisms. *Adv. Funct. Mater.* **2012**, *22*, 849−854.
(32) Ide, Y.; Matsuoka, M.; Ogawa, M. Efficient Visible-Light-Induced Photocatalytic Activity on Gold-Nanoparticle-Supported Layered Titanate. *J. Am. Chem. Soc.* **2010**, *132*, 16762−16764.
(33) Primo, A.; Corma, A.; Garcia, H. Titania Supported Gold Nanoparticles as Photocatalyst. *Phys. Chem. Chem. Phys.* **2011**, *13*, 886−910.
(34) Zhu, S. Y.; Liang, S. J.; Gu, Q.; Xie, L. Y.; Wang, J. X.; Ding, Z. X.; Liu, P. Effect of Au Supported TiO_2 with Dominant Exposed {001} Facets on the Visible-Light Photocatalytic Activity. *Appl. Catal., B* **2012**, *119*, 146−155.
(35) Lee, J.; Mubeen, S.; Ji, X. L.; Stucky, G. D.; Moskovits, M. Plasmonic Photoanodes for Solar Water Splitting with Visible Light. *Nano Lett.* **2012**, *12*, 5014−5019.
(36) Wang, P.; Huang, B. B.; Dai, Y.; Whangbo, M. H. Plasmonic Photocatalysts: Harvesting Visible Light with Noble Metal Nanoparticles. *Phys. Chem. Chem. Phys.* **2012**, *14*, 9813−9825.
(37) Sarina, S.; Waclawik, E. R.; Zhu, H. Y. Photocatalysis on Supported Gold and Silver Nanoparticles under Ultraviolet and Visible Light Irradiation. *Green Chem.* **2013**, *15*, 1814−1833.
(38) Feng, Y. H.; Yin, H. B.; Gao, D. Z.; Wang, A. L.; Shen, L. Q.; Meng, M. J. Selective Oxidation of 1,2-Propanediol to Lactic Acid Catalyzed by Hydroxylapatite Nanorod-Supported Au/Pd Bimetallic Nanoparticles under Atmospheric Pressure. *J. Catal.* **2014**, *316*, 67−77.
(39) Ryabenkova, Y.; He, Q.; Miedziak, P. J.; Dummer, N. F.; Taylor, S. H.; Carley, A. F.; Morgan, D. J.; Dimitratos, N.; Willock, D. J.; Bethell, D.; Knight, D. W.; Chadwick, D.; Kiely, C. J.; Hutchings, G. J. The Selective Oxidation of 1,2-Propanediol to Lactic Acid using Mild Conditions and Gold-Based Nanoparticulate Catalysts. *Catal. Today* **2013**, *203*, 139−145.
(40) Yan, S. C.; Li, Z. S.; Zou, Z. G. Photodegradation Performance of g-C_3N_4 Fabricated by Directly Heating Melamine. *Langmuir* **2009**, *25*, 10397−10401.
(41) Liu, J. H.; Zhang, T. K.; Wang, Z. C.; Dawson, G.; Chen, W. Simple Pyrolysis of Urea into Graphitic Carbon Nitride with Recyclable Adsorption and Photocatalytic Activity. *J. Mater. Chem.* **2011**, *21*, 14398−14401.
(42) Sun, J. X.; Yuan, Y. P.; Qiu, L. G.; Jiang, X.; Xie, A. J.; Shen, Y. H.; Zhu, J. F. Fabrication of Composite Photocatalyst g-C_3N_4-ZnO and Enhancement of Photocatalytic Activity under Visible Light. *Dalton Trans.* **2012**, *41*, 6756−6763.
(43) Sun, X. P.; Dong, S. J.; Wang, E. Large-Scale Synthesis of Micrometer-Scale Single-Crystalline Au Plates of Nanometer Thickness by a Wet-Chemical Route. *Angew. Chem., Int. Ed.* **2004**, *43*, 6360−6363.
(44) Zhang, Z. Y.; Wang, Z.; Cao, S. W.; Xue, C. Au/Pt Nanoparticle-Decorated TiO_2 Nanofibers with Plasmon-Enhanced Photocatalytic Activities for Solar-to-Fuel Conversion. *J. Phys. Chem. C* **2013**, *117*, 25939−25947.
(45) Zhu, Y. P.; Li, M.; Liu, Y. L.; Ren, T. Z.; Yuan, Z. Y. Carbon-Doped ZnO Hybridized Homogeneously with Graphitic Carbon

DOI: 10.1021/acsami.5b01212
ACS Appl. Mater. Interfaces 2015, 7, 9630−9637

Nitride Nanocomposites for Photocatalysis. *J. Phys. Chem. C* **2014**, *118*, 10963−10971.
(46) Deng, Q. F.; Liu, L.; Lin, X. Z.; Du, G. H.; Liu, Y. P.; Yuan, Z. Y. Synthesis and CO_2 Capture Properties of Mesoporous Carbon Nitride Materials. *Chem. Eng. J.* **2012**, *203*, 63−70.
(47) Dong, F.; Wu, L. W.; Sun, Y. J.; Fu, M.; Wu, Z. B.; Lee, S. C. Efficient Synthesis of Polymeric g-C_3N_4 Layered Materials as Novel Efficient Visible Light Driven Photocatalysts. *J. Mater. Chem.* **2011**, *21*, 15171−15174.
(48) Zhang, P.; Shao, C. L.; Li, X. H.; Zhang, M. Y.; Zhang, X.; Sun, Y. Y.; Liu, Y. C. In Situ Assembly of Well-Dispersed Au Nanoparticles on TiO_2/ZnO Nanofibers: A Three-Way Synergistic Heterostructure with Enhanced Photocatalytic Activity. *J. Hazard. Mater.* **2012**, *237*, 331−338.
(49) Chai, B.; Peng, T. Y.; Zeng, P.; Mao, J. Synthesis of Floriated In_2S_3 Decorated with TiO_2 Nanoparticles for EfficientPhotocatalytic Hydrogen Production under Visible Light. *J. Mater. Chem.* **2011**, *21*, 14587−14593.
(50) Jang, J. S.; Choi, S. H.; Kim, H. G.; Lee, J. S. Location and State of Pt in Platinized CdS/TiO_2 Photocatalysts for Hydrogen Production from Water under Visible Light. *J. Phys. Chem. C* **2008**, *112*, 17200−17205.
(51) Dong, R. F.; Tian, B. Z.; Zeng, C. Y.; Li, T. Y.; Wang, T. T.; Zhang, J. L. Ecofriendly Synthesis and Photocatalytic Activity of Uniform Cubic Ag@AgCl Plasmonic Photocatalyst. *J. Phys. Chem. C* **2013**, *117*, 213−220.
(52) Singh, G. P.; Shrestha, K. M.; Nepal, A.; Klabunde, K. J.; Sorensen, C. M. Graphene Supported Plasmonic Photocatalyst for Hydrogen Evolution in Photocatalytic Water Splitting. *Nanotechnology* **2014**, *25*, 265701.
(53) Yonezawa, T.; Matsune, H.; Kunitake, T. Layered Nanocomposite of Close-Packed Gold Nanoparticles and TiO_2 Gel Layers. *Chem. Mater.* **1999**, *11* (1), 33−35.
(54) Della Gaspera, E.; Bersani, M.; Mattei, G.; Nguyen, T. L.; Mulvaney, P.; Martucci, A. Cooperative Effect of Au and Pt Inside TiO_2 matrix for Optical Hydrogen Detection at Room Temperature Using Surface Plasmon Spectroscopy. *Nanoscale* **2012**, *4*, 5972−5979.
(55) Sarmah, A. K.; Meyer, M. T.; Boxall, A. B. A. A Global Perspective on the Use, Sales, Exposure Pathways, Occurrence, Fate and Effects of Veterinary Antibiotics (VAs) in the Environment. *Chemosphere* **2006**, *65*, 725−759.
(56) Wang, X. H.; Li, J. G.; Kamiyama, H.; Moriyoshi, Y.; Ishigaki, T. Wavelength-Sensitive Photocatalytic Degradation of Methyl Orange in Aqueous Suspension over Iron(III)-Doped TiO_2 Nanopowders under UV and Visible Light Irradiation. *J. Phys. Chem. B* **2006**, *110*, 6804−6809.
(57) Zhang, Z. Y.; Li, A. R.; Cao, S. W.; Bosman, M.; Li, S. Z.; Xue, C. Direct Evidence of Plasmon Enhancement on Photocatalytic Hydrogen Generation over Au/Pt-Decorated TiO_2 Nanofibers. *Nanoscale* **2014**, *6*, 5217−5222.
(58) Mubeen, S.; Lee, J.; Singh, N.; Kramer, S.; Stucky, G. D.; Moskovits, M. An Autonomous Photosynthetic Device in Which All Charge Carriers Derive from Surface Plasmons. *Nat. Nanotechnol.* **2013**, *8*, 247−251.
(59) Zhang, X.; Liu, Y.; Lee, S. T.; Yang, S. H.; Kang, Z. H. Coupling Surface Plasmon Resonance of Gold Nanoparticles with Slow-Photon-Effect of TiO_2 Photonic Crystals for Synergistically Enhanced Photoelectrochemical Water Splitting. *Energy Environ. Sci.* **2014**, *7*, 1409−1419.
(60) An, Y. R.; Tang, L. L.; Jiang, X. L.; Chen, H.; Yang, M. C.; Jin, L. T.; Zhang, S. P.; Wang, C. G.; Zhang, W. A Photoelectrochemical Immunosensor Based on Au-Doped TiO_2 Nanotube Arrays for the Detection of Alpha-Synuclein. *Chem.—Eur. J.* **2010**, *16*, 14439−14446.
(61) Atienzar, P.; Ishwara, T.; Illy, B. N.; Ryan, M. P.; O'Regan, B. C.; Durrant, J. R.; Nelson, J. Control of Photocurrent Generation in Polymer/ZnO Nanorod Solar Cells by Using a Solution-Processed TiO_2 Overlayer. *J. Phys. Chem. Lett.* **2010**, *1*, 708−713.
(62) Guo, C. X.; Yang, H. B.; Sheng, Z. M.; Lu, Z. S.; Song, Q. L.; Li, C. M. Layered Graphene/Quantum Dots for Photovoltaic Devices. *Angew. Chem., Int. Ed.* **2010**, *49*, 3014−3017.
(63) Ren, H. T.; Jia, S. Y.; Wu, Y.; Wu, S. H.; Zhang, T. H.; Han, X. Improved Photochemical Reactivities of Ag_2O/g-C_3N_4 in Phenol Degradation under UV and Visible Light. *Ind. Eng. Chem. Res.* **2014**, *53*, 17645−17653.
(64) Xu, M.; Han, L.; Dong, S. J. Facile Fabrication of Highly Efficient g-C_3N_4/Ag_2O Heterostructured Photocatalysts with Enhanced Visible-Light Photocatalytic Activity. *ACS Appl. Mater. Interfaces* **2013**, *5*, 12533−12540.
(65) Zhang, Y. F.; Mao, F.; Yan, H. J.; Liu, K. W.; Cao, H. M.; Wu, J. G.; Xiao, D. Q. A Polymer-Metal-Polymer-Metal Heterostructure for Enhanced Photocatalytic Hydrogen Production. *J. Mater. Chem. A* **2015**, *3*, 109−115.

DOI: 10.1021/acsami.5b01212
ACS Appl. Mater. Interfaces 2015, 7, 9630−9637